nature astronomy

Article https://doi.org/10.1038/s41550-024-02249-0

Identification of the weak-to-strong transition in Alfvénic turbulence from space plasma

In the format provided by the authors and unedited

Supplementary information

Deviations between the mean magnetic field and local field

The anisotropy of Alfvénic fluctuations depends on the local background magnetic field. Although it would be better to use a scale-dependent mean magnetic field ideally, the mode decomposition method is based on a perturbative treatment of fluctuations in the presence of a uniform magnetic field ($\mathbf{B}_0$). This method requires $\mathbf{B}_0$ independent of the transformation between real and wavevector space. Nevertheless, Supplementary Fig. 1 shows the spacecraft-frame frequency-time spectrum of the cosine of angle ($|cos\langle\mathbf{B}_0, \mathbf{B}_{local}\rangle|$) between $\mathbf{B_0}$ and $\mathbf{B}_{local}$. The local mean field is calculated as $\mathbf{B}_{local} = [\mathbf{B}(t-2\tau)+4\mathbf{B}(t-\tau)+6\mathbf{B}(t)+4\mathbf{B}(t+\tau)+\mathbf{B}(t+2\tau)]/16$, where τ is the timescale. The mean magnetic field ($\mathbf{B}_0$) within a five-hour moving time window is closely aligned with $\mathbf{B}_{local}$, suggesting that $\mathbf{B}_0$ approximating the local mean field is acceptable.

Two-dimensional energy wavenumber distributions at different time window lengths

To further address this limitation of the mode decomposition method, this study explores the variation of two-dimensional (2D) wavenumber distributions of Alfvénic magnetic energy $D_{B_A}(k_\perp, k_\parallel)$ by adjusting the length of time windows, where

$$D_{B_A}(k_\perp, k_\parallel) = \int_0^\infty P_{B_A}(k_\perp, k_\parallel, f_{sc}) df_{sc}. \tag{1}$$

We show magnetic energy spectra with different time window lengths in Supplementary Fig. 2. To simplify, the modeled theoretical energy spectra ($I_A(k_\perp, k_\parallel)$) are estimated with the same parameters ($M_{A,turb} \sim 0.33$, $L_0 \sim 4.6 \times 10^4 km$). (i) The longer time window length provides more low-frequency (large-scale) measurements. (ii) Energy spectra with shorter time window lengths are more consistent with theoretical contours in the strong turbulence regime (at larger $k_\perp$). It is likely because the mean magnetic field in shorter time windows is closer to the local mean field of fluctuations with larger wavenumbers. (iii) The main changes in energy distributions are little affected by time window length: $k_\parallel$ distributions of magnetic energy start to broaden around $k_\perp > 2 \times 10^{-4} km^{-1}$ for all panels.

We show the results with a five-hour length in the main text for two reasons: (i) The length cannot be too long. The shorter the window length, the closer to the local background magnetic field. (ii) The length cannot be too short in order to ensure the measurements of low-frequency (large-scale) signals since the Alfvénic weak-to-strong transition is present on relatively large scales. The five-hour length selection provides the low-frequency (large-scale) measurements while ensuring $\mathbf{B}_0$ is approaching the local background magnetic field.

Details of examination of the turbulence state

To examine the turbulent state, we calculate the normalized correlation function $R(\tau)/R(0)$, where the correlation function is defined as $R(\tau) = \langle \delta B(t)\delta B(t+\tau)\rangle$, τ is the timescale, and angular brackets are a time average over the time window length (5 hours). Supplementary Fig. 3 shows $R(\tau)/R(0)$ for magnetic field $\delta B_{\perp 1}$ and $\delta B_{\perp 2}$ components in field-aligned coordinates. Fluctuations $\delta B_{\perp 1}$ are in $(\hat{\mathbf{b}}_0 \times \hat{\mathbf{X}}_{GSE}) \times \hat{\mathbf{b}}_0$ directions, and $\delta B_{\perp 2}$ are in $\hat{\mathbf{b}}_0 \times \hat{\mathbf{X}}_{GSE}$ directions, where $\hat{\mathbf{X}}_{GSE}$ is the unit vector towards the Sun from the Earth.

This study estimates the correlation time $T_c \sim \int_0^{R(\tau)\to\frac{1}{2e}} R(\tau)/R(0)d\tau$. In Supplementary Fig. 3, $T_c \sim [1300, 2300]s$ is much less than the time window length (5 hours), suggesting that fluctuations are approximately stationary. Moreover, $R(\tau)/R(0)$ profiles in all time windows are similar, suggesting that the starting time of the moving time window has a slight influence on $R(\tau)/R(0)$, and thus fluctuations are homogeneous. Above all, it is reasonable to describe structures of turbulent fluctuations using three-dimensional energy distributions.

Schematic of Alfvén mode decomposition from turbulent fluctuations

Supplementary Fig. 4 shows a coordinate determined by unit vectors of the wavevector and background magnetic field ($\hat{\mathbf{k}}_{SVD}$ and $\hat{\mathbf{b}}_0$). The basis vectors of coordinate axes are in $\hat{\mathbf{b}}_0$, $\hat{\mathbf{k}}_{\perp,outof(k_{SVD},b_0)plane} = \frac{\hat{\mathbf{k}}_{SVD}\times\hat{\mathbf{b}}_0}{|\hat{\mathbf{k}}_{SVD}\times\hat{\mathbf{b}}_0|}$, and $\hat{\mathbf{k}}_{\perp,in(k_{SVD},b_0)plane} = \hat{\mathbf{b}}_0 \times \hat{\mathbf{k}}_{\perp,outof(k_{SVD},b_0)plane}$ directions. Alfvénic magnetic field and velocity fluctuations are along $\hat{\xi}_A$ direction, where $\hat{\xi}_A = \hat{\mathbf{k}}_{\perp,outof(k_{SVD},b_0)plane}$. The wavevectors ($\mathbf{k}_A$) calculated by multispacecraft timing analysis on Alfvénic magnetic field are not completely alighted with $\hat{\mathbf{k}}_{SVD}$. Thus, we set the angle η between $\mathbf{k}_A$ and $\hat{\mathbf{k}}_{SVD}$ as a threshold and only analyze the fluctuations inside the cone.

One-dimensional and two-dimensional wavenumber distributions of Alfvénic energy

One-dimensional (1D) wavenumber distributions of Alfvénic magnetic energy are calculated by

$$D_{B_A}(k_\perp) = \sum_{k_\parallel=0}^{k_\parallel\to\infty} \int_0^\infty P_{B_A}(k_\perp, k_\parallel, f_{sc})df_{sc}, \tag{2}$$

$$D_{B_A}(k_\parallel) = \sum_{k_\perp=0}^{k_\perp\to\infty} \int_0^\infty P_{B_A}(k_\perp, k_\parallel, f_{sc})df_{sc}. \tag{3}$$

In Supplementary Fig. 5, 1D wavenumber distributions of Alfvénic magnetic energy from data sets under different η limits nearly overlap both for $D_{B_A}(k_\perp)$ and $D_{B_A}(k_\parallel)$, where η is the angle between $\mathbf{k}_{SVD}$ and $\mathbf{k}_A$ (Supplementary Fig. 4). Due to the limited data samples, 1D wavenumber distributions from data sets with $\eta < 10°$ and $\eta < 15°$

show significant deviations from others in Supplementary Fig. 5, and more vacant bins exhibit in 2D wavenumber distributions under smaller η in Supplementary Fig. 6. More data samples are involved with the relaxation of η limits. On the whole, Alfvénic magnetic energy using data sets under different η limits shows similar distributions in Supplementary Figs. 5 and 6.

Energy spectra and nonlinear parameters with velocity measurements

We observe a similar Alfvénic weak-to-strong transition with the measurements of proton velocity fluctuations. The energy spectral density of Alfvénic velocity is defined as $E_{V_A}(k_\perp) = \frac{\delta V_A^2(k_\perp)}{2k_\perp}$, where the Alfvénic velocity energy density is calculated by $\delta V_A^2(k_\perp) = 2\sum_{k_\perp=k_\perp}^{k_\perp\to\infty}\sum_{k_\parallel=0}^{k_\parallel\to\infty}\int_0^\infty P_{V_A}(k_\perp, k_\parallel, f_{sc})df_{sc}$. Supplementary Fig. 7a shows the sharp change in spectral slopes of $E_{V_A}(k_\perp)$ from wave-like (-2) to Kolmogorov-like $(-5/3)$. In Supplementary Fig. 7b, for most of the data points, $k_\parallel$ is approximately stable within $k_\parallel \sim [7\times10^{-5}, 1\times10^{-4}]km^{-1}$ in Zone (1), whereas the variation of $k_\perp$ versus $k_\parallel$ agrees with the scaling $k_\parallel \propto k_\perp^{2/3}$ in Zone (3). The nonlinearity parameter is estimated as $\chi_{V_A}(k_\perp, k_\parallel) = \frac{k_\perp \delta V_A(k_\perp, k_\parallel)}{k_\parallel V_A}$, where the Alfvénic velocity energy density is estimated by $\delta V_A^2(k_\perp, k_\parallel) = \sum_{k_\perp=k_\perp}^{k_\perp\to\infty}\sum_{k_\parallel=k_\parallel}^{k_\parallel\to\infty}\int_0^\infty P_{V_A}(k_\perp, k_\parallel, f_{sc})df_{sc}$. Supplementary Fig. 7c shows that, at the corresponding wavenumbers in Supplementary Fig. 7b, χ_{V_A} is much less than unity in Zone (1), whereas χ_{V_A} increases approaching unity and follows the scaling $k_\parallel \propto k_\perp^{2/3}$ in Zone (3).

Summary of methodology limitation

(1) This study is restricted to Alfvénic fluctuations at small amplitude, excluding 2D modes (see Main text).
(2) This study is limited by ion characteristic scales and satellite relative separations $(1/(100d_{sc}) < k < min(0.1/max(d_i, r_{ci}), \pi/d_{sc})$; see Methods).
(3) This study examines stationary and homogeneous fluctuations, excluding any involvement in turbulence evolution processes (Supplementary information).

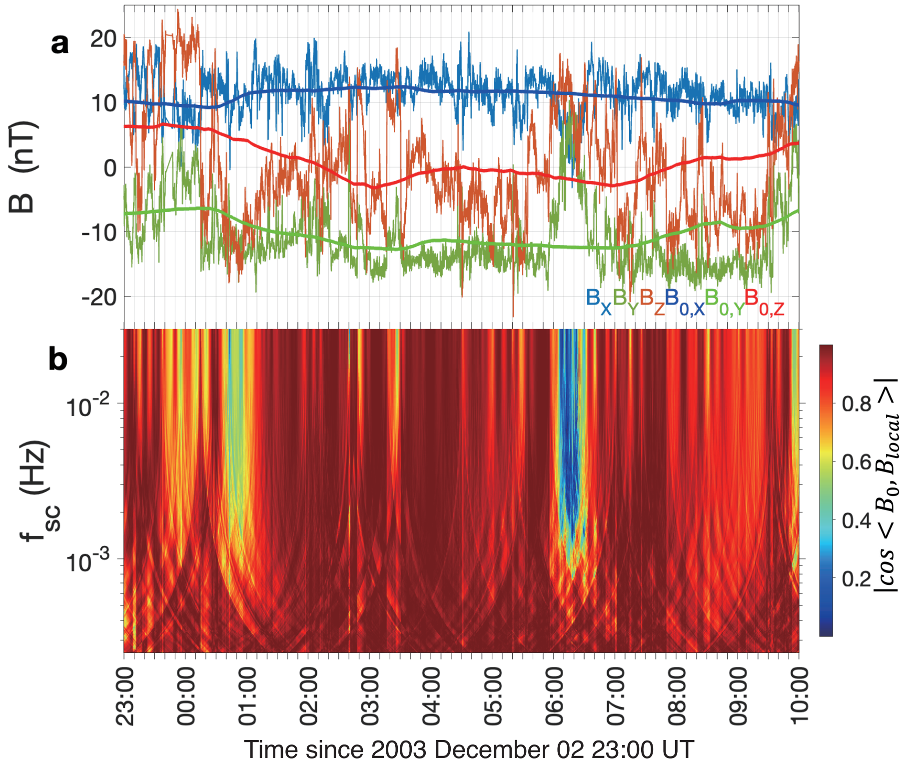

Supplementary Fig. 1 Deviations between the mean magnetic field and local field. **a**, Time series of magnetic field ($\mathbf{B} = [B_X, B_Y, B_Z]$) and mean magnetic field components ($\mathbf{B_0} = [B_{0,X}, B_{0,Y}, B_{0,Z}]$). **b**, The spacecraft-frame frequency-time spectrum of the cosine of angle ($|cos\langle \mathbf{B}_0, \mathbf{B}_{local}\rangle|$) between $\mathbf{B_0}$ and $\mathbf{B}_{local}$. $\mathbf{B_0}$ is the mean magnetic field within a five-hour moving time window, and $\mathbf{B}_{local}$ is the local mean magnetic field.

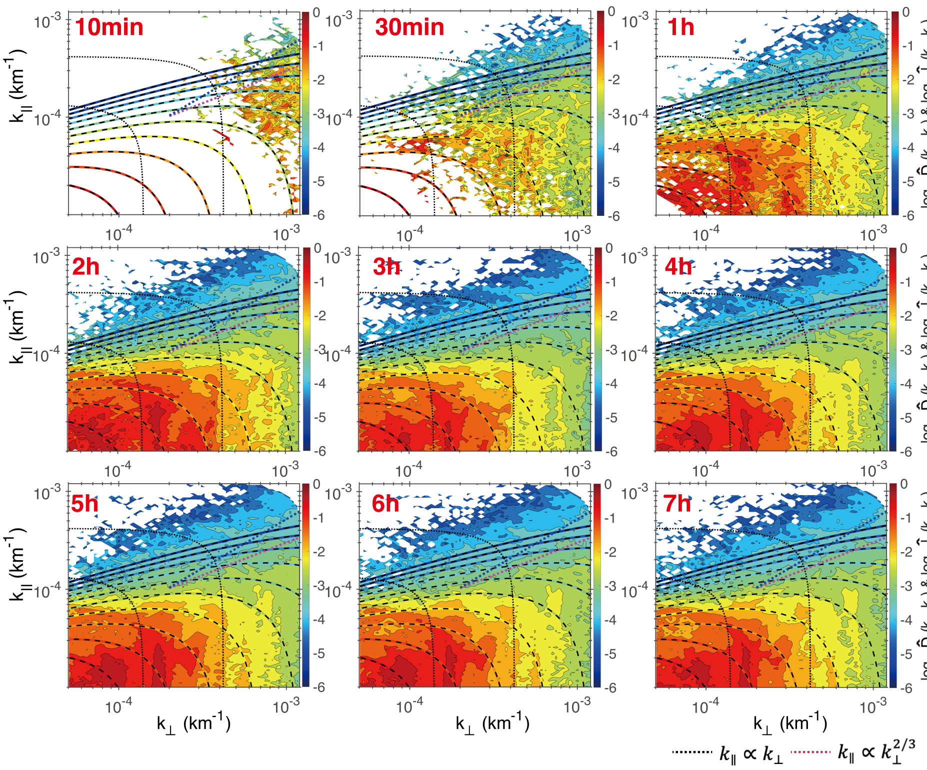

Supplementary Fig. 2 The comparisons between wavenumber distributions of Alfvénic magnetic energy $\hat{D}_{B_A}(k_\perp, k_\parallel)$ and theoretical energy spectra $\hat{I}_A(k_\perp, k_\parallel)$. All panels utilize the same format as Fig. 2b in the main text using the data sets under $\eta < 30°$. $\hat{D}_{B_A}(k_\perp, k_\parallel)$ is displayed by the filled 2D color contours. $\hat{I}_A(k_\perp, k_\parallel)$ is displayed by color contours with black dashed curves. The time in the upper left corner of each panel represents the length of the time window. The dotted curves mark $k = \sqrt{k_\parallel^2 + k_\perp^2} = 0.01/d_i$ and $0.03/d_i$.

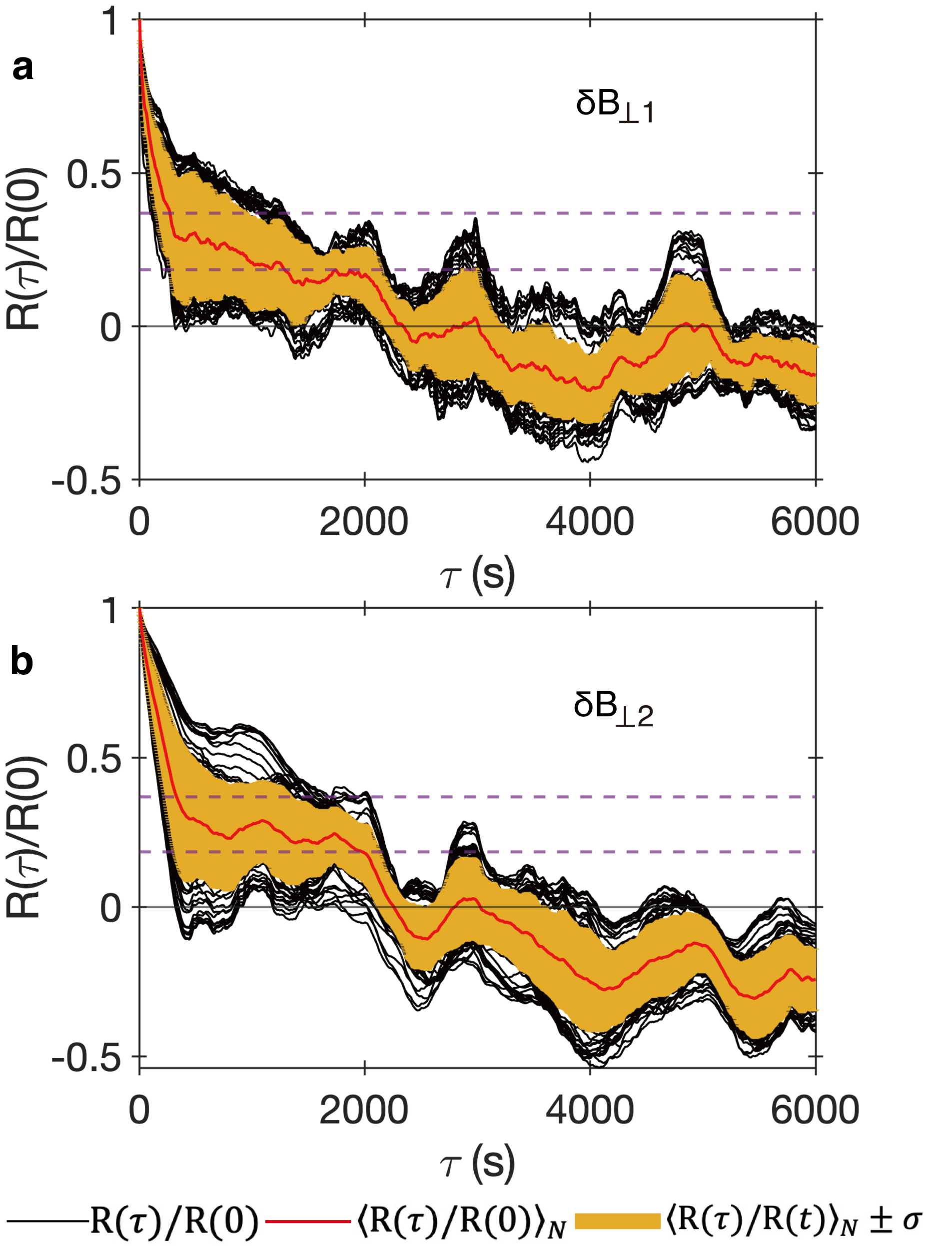

Supplementary Fig. 3 Normalized correlation functions ($R(\tau)/R(0)$) versus timescale (τ) in field-aligned coordinates. **a**,**b**, $R(\tau)/R(0)$ versus τ for $\delta B_{\perp 1}$ and $\delta B_{\perp 2}$. The solid curves represent $R(\tau)/R(0)$ and average $R(\tau)/R(0)$ ($\langle R(\tau)/R(0)\rangle_N$), and the shaded regions represent $[\langle R(\tau)/R(0)\rangle_N - \sigma, \langle R(\tau)/R(0)\rangle_N + \sigma]$, where σ is standard deviations of $R(\tau)/R(0)$ with the window number $N = 73$. The horizontal dashed lines represent $R(\tau)/R(0) = 1/e$ and $1/(2e)$.

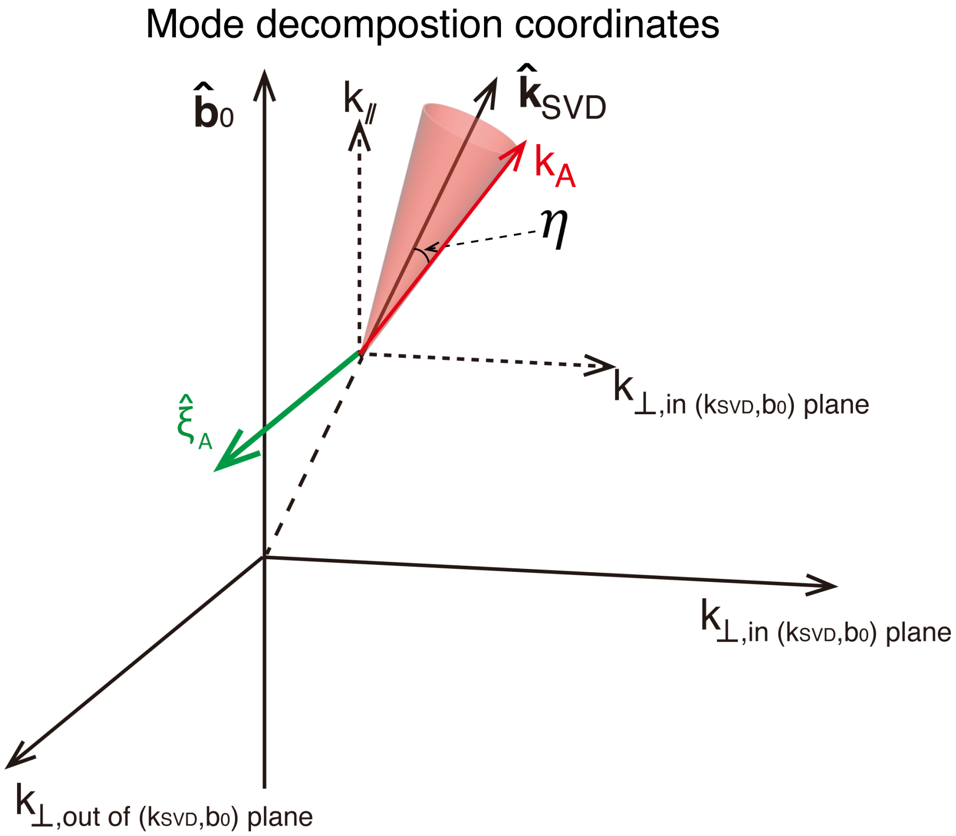

Supplementary Fig. 4 Schematic of Alfvén mode decomposition from fluctuations. The coordinates are determined by $\hat{\mathbf{b}}_0$ and $\hat{\mathbf{k}}_{SVD}$. The Alfvénic displacement vector $\hat{\xi}_A$ is displayed by the arrow along the direction out of (k_{SVD}, b_0) plane. The cone marks all $\mathbf{k}_A$ that make an angle η with $\hat{\mathbf{k}}_{SVD}$.

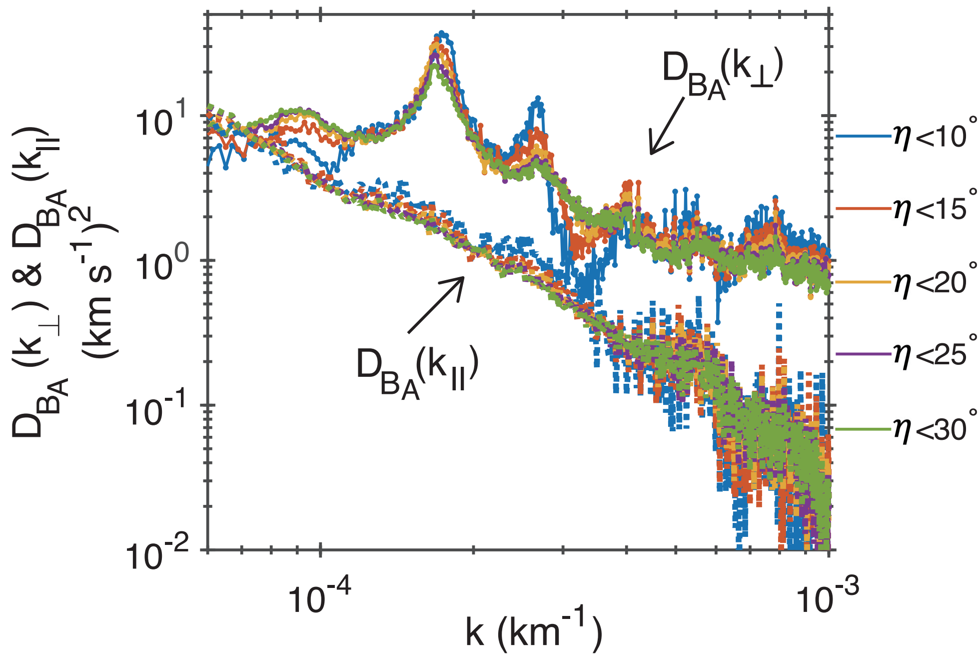

Supplementary Fig. 5 1D wavenumber distributions of Alfvénic magnetic energy using data sets under $\eta < 10°$, $15°$, $20°$, $25°$, and $30°$. $D_{B_A}(k_\perp)$ is displayed by solid curves. $D_{B_A}(k_\parallel)$ is displayed by dotted curves.

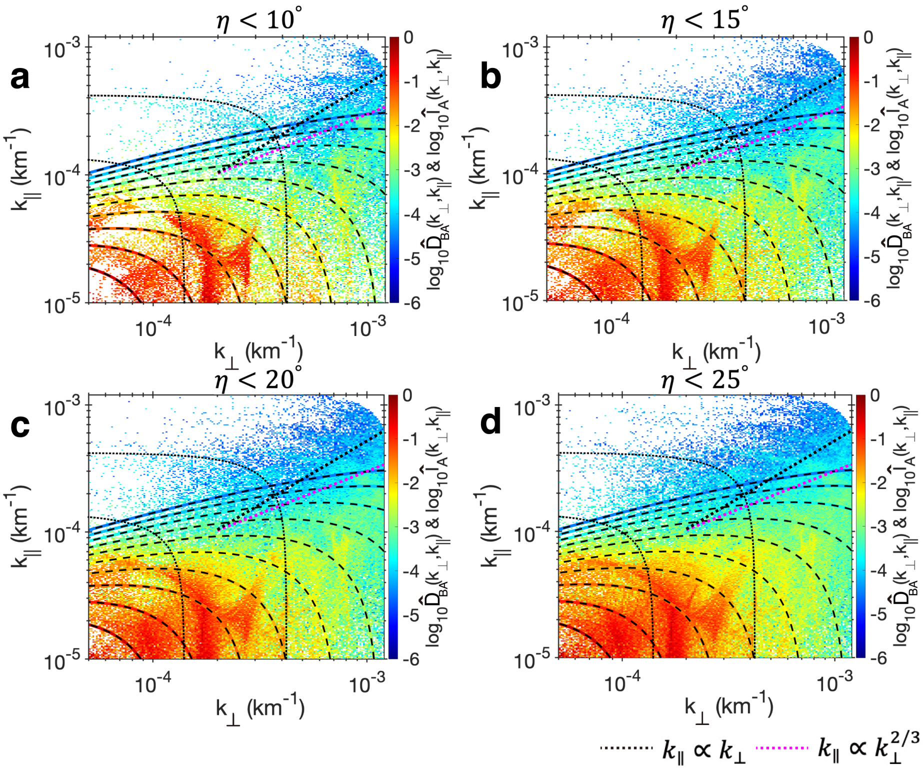

Supplementary Fig. 6 2D wavenumber distributions of Alfvénic magnetic energy using data sets under $\eta < 10°$, $15°$, $20°$, and $25°$. For each panel, use the same format as Fig. 2a in the main text. The 2D spectral image represents $\hat{D}_{B_A}(k_\perp, k_\parallel)$. The color contours with black dashed curves represent $\hat{I}_{B_A}(k_\perp, k_\parallel)$, which is in the same color map as $\hat{D}_{B_A}(k_\perp, k_\parallel)$. The dotted curves mark $k = \sqrt{k_\parallel^2 + k_\perp^2} = 0.01/d_i$ and $0.03/d_i$.

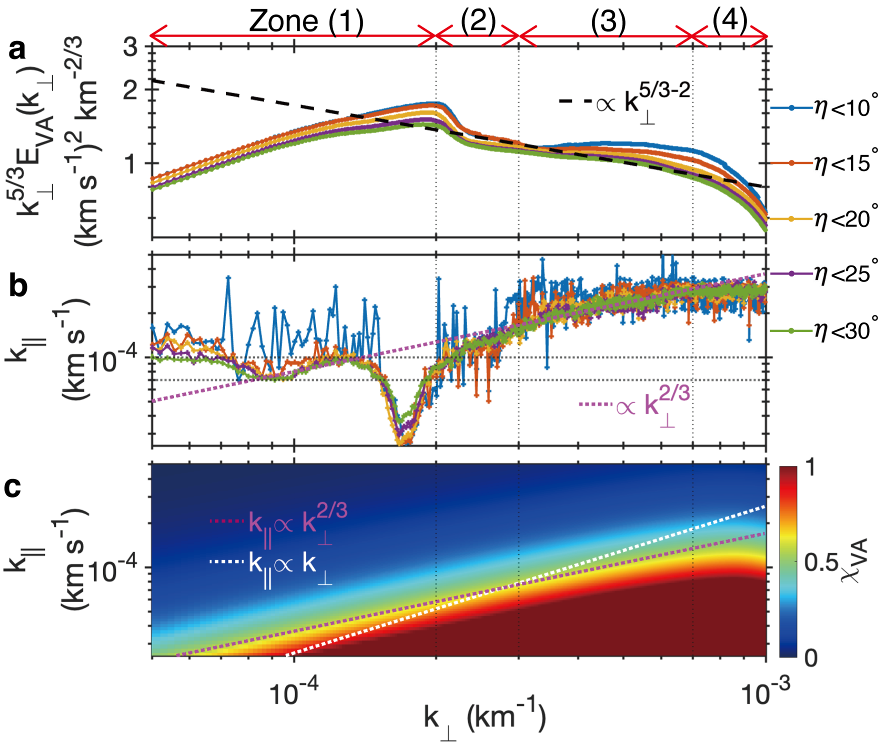

Supplementary Fig. 7 Perpendicular wavenumber dependence of the compensated spectra ($k_\perp^{5/3}E_{V_A}(k_\perp)$), parallel wavenumber ($k_\parallel$), and nonlinearity parameter ($\chi_{V_A}(k_\perp, k_\parallel)$). **a**, $k_\perp^{5/3}E_{V_A}(k_\perp)$ are displayed by curves. The dashed line represents the scaling $k_\perp^{5/3}E_{V_A}(k_\perp) \propto k_\perp^{5/3-2}$. **b**, The variation of $k_\parallel$ versus $k_\perp$ by taking the same values of proton velocity energy. The dotted line represents the scaling $k_\parallel \propto k_\perp^{2/3}$. The horizontal dotted lines mark $k_\parallel = 7 \times 10^{-5} km^{-1}$ and $10^{-4} km^{-1}$. **c**, $\chi_{V_A}(k_\perp, k_\parallel)$ spectrum calculated using the data set under $\eta < 30°$. The $k_\perp$ dependence figure is divided into four zones: (1) $5 \times 10^{-5} < k_\perp < 2 \times 10^{-4} km^{-1}$, (2) $2 \times 10^{-4} < k_\perp < 3 \times 10^{-4} km^{-1}$, (3) $3 \times 10^{-4} < k_\perp < 7 \times 10^{-4} km^{-1}$, and (4) $7 \times 10^{-4} < k_\perp < 1 \times 10^{-3} km^{-1}$. The first, second, and third vertical dotted lines are around the maximum of $k_\perp^{5/3}E_{V_A}(k_\perp)$, the beginning and the end of flattened $k_\perp^{5/3}E_{V_A}(k_\perp)$, respectively.